RESEARCH ARTICLE
doi: 10.2306/scienceasia1513-1874.2026.025

ScienceAsia 52 (1): 2026: ID 2026025: **1–10**

Microbial fermentation of corn stalks by *Streptomyces rochei se-93*: Extraction, characterization and hypoglycemic function assessment of polysaccharides

Shuwei Li[a], Meitong Li[b,c,d], Jinmi Wu[a], Xuening Fei[a], Jinjun Yang[a], Yuhong Xie[a,*], Huimin Huo[e,*]

[a] School of Environmental Science and Safety Engineering, Tianjin University of Technology, Tianjin 300384 China
[b] School of Chemistry and Chemical Engineering, Tianjin University of Technology, Tianjin 300384 China
[c] Tianjin Key Laboratory of Hazardous Waste Safety Disposal and Recycling Technology, Tianjin 300384 China
[d] Tianjin Engineering Research Center of Green Chemical Industry and Waste Recycling, Tianjin 300384 China
[e] Solid Waste and Chemicals Management Center, Ministry of Ecology and Environment of the People's Republic of China, 100029 China

*Corresponding authors, e-mail: xieyuhong76@126.com, huohuimin@meescc.cn
Received 30 May 2025, Accepted 5 Mar 2026
Available online 22 Mar 2026

ABSTRACT: The effective utilization of straw is one of the pathways for the green and sustainable development of agriculture. This study utilized *Streptomyces rochei se-93* for the liquid-state fermentation of corn stalks yielding polysaccharide products which were extensively characterized. Our results demonstrate that inoculation with *S. rochei se-93* significantly enhanced the polysaccharide content in the fermentation broth and promoted the degradation of cellulose, hemicellulose, and lignin in corn stalks. The fermentation by *S. rochei se-93* did not alter the monosaccharide composition, configuration, or functional groups of the polysaccharides, but it did modify the monosaccharide composition ratio and reduce the thermal stability of the polysaccharides. Meanwhile, fermentation significantly improved the hypoglycemic activity of the polysaccharides: at a concentration of 2 mg/ml, its inhibition rate against α-amylase reached 56.90 ± 0.42%, which was approximately 4.50% higher than that of the control group CSP-B (54.43 ± 0.28% at 4 mg/ml); at a concentration of 10 mg/ml, its inhibition rate against α-glucosidase reached 83.40 ± 1.36%, representing an approximate 10.96% increase compared to CSP-B (75.16 ± 0.91%). This study contributes to the high-value utilization of agricultural waste (corn stalks) and offers a potential pathway for developing novel natural compounds with hypoglycemic properties.

KEYWORDS: corn stalk, polysaccharides, hypoglycemic activity

INTRODUCTION

Crop residues are diverse and abundant. Corn stalks contain a rich amount of polysaccharides. By extracting these polysaccharides, not only can the environmental threats posed by the residues be reduced, but considerable economic benefits can also be achieved. Polysaccharides from natural sources have been confirmed to possess various biological activities and application potential in the field of food and medicine, for example, *Chimonanthus salicifolius* polysaccharide was found to exert a significant protective effect on acute alcoholic liver injury in mice through relevant mechanisms [1] Actinomycetes are superior straw-degrading strains due to their abundant mycelium and conidia production, stronger lignocellulose degradation capability than bacteria, and greater environmental adaptability than fungi [2, 3].

Streptomyces rochei is a Gram-positive actinobacterium with efficient crop straw-degrading capacity [4]. Current studies on straw degradation by *S. rochei* are primarily focused on the screening of strains, investigations into degradation rates of different straw components, evaluation of degradation efficiency along with optimization of conditions, and analysis of structural and property modifications caused by fermentation.

For example, Gong et al [5] isolated three lignocellulose-degrading strains—*S.* sp.
G1, G2, and G3—from soils in cold regions. Zhang et al [3] isolated and purified *S. rochei ZY-2* with high lignocellulosic degradation capabilities from straw compost and forest soil, achieving a degradation rate of 29.23% on rice straw within 7 days. Wang et al [6] showed that *S. rochei* degraded different parts of wheat straw at varying rates in flooded conditions, with the highest degradation rate observed in leaves, followed by leaf sheaths, spikelets, and roots, while the degradation rate of wheat straw stems was the slowest. Jin et al [7] and colleagues investigated the effects of carbon-to-nitrogen ratio, inoculum size, and fermentation time on the degradation rate of rice straw by *S. rochei* during fermentation and analyzed the changes in the rheological properties of the rice straw after aerobic fermentation.

However, there were currently no research data on the analysis of the products after the fermentation of straw by *S. rochei*. This study utilizes *S. rochei* to degrade corn stalk and investigated the polysaccharide products in the fermentation broth, aiming to provide a new pathway for the high-value utilization of corn stalk.

Table 1 Composition of the fermentation medium

Name of culture medium	Component	Dosage (g/l)
Fermentation medium	K_2HPO_4	1.0
	$NaNO_3$	2.5
	$MgSO_4 \cdot 7H_2O$	0.3
	NaCl	0.1
	$CaCl_2$	0.1
	$FeCl_3$	0.01
	$CaCO_3$	2.0
	Corn stalks	50.0

Note: pH 7.2∼7.4, 121 °C sterilization for 30 min, for later use.

MATERIALS AND METHODS

Experimental strain

Streptomyces rochei se-93 with high-efficiency corn stalk-degrading capability, isolated by the Microbiology Laboratory of Tianjin University of Technology, was preserved at the China General Microbiological Culture Collection Center under the accession number CGMCC No. 18291.

Experimental materials

The key instruments and their sources are as follows: High Performance Liquid Chromatography (HPLC) from Shimadzu (Kyoto, Japan); Atomic Force Microscopy (AFM) and Fourier Transform Infrared Spectrometer (FTIR) from Bruker (Karlsruhe, Germany); Scanning Electron Microscopy (SEM) from FEI Company (Hillsboro, USA); and Thermal Gravimetric Analyzer (TGA) from TA Instruments (New Castle, USA).

α-Amylase (50 U/mg) was purchased from Shanghai Macklin Biochemical Technology Co., Ltd., China; α-glucosidase (50 U/mg) was obtained from Shanghai Yuanye Bio-Technology Co., Ltd., China.

Corn stalks were cut into segments approximately 3 cm long using scissors, dried at 60 °C, and then pulverized with a grinder. The resulting material was sieved through an 80-mesh screen, and the undersize fraction was collected. This fraction was mixed with water at a mass ratio of 1:30 (water:corn stalks), heated in a water bath at 80 °C for 2 h, and then subjected to suction filtration. The filter residue was collected, dried in an oven at 60 °C, and finally stored as corn stalk powder in a dry environment for future use.

The main types and formulations of culture media used in this experiment were shown in Table 1.

Experimental methods

Fermentation

4% (v/v) of *S. rochei se-93* culture broth was inoculated into a 200 ml fermentation medium and incubated at 30 °C with shaking at 120 rpm for 12 d. Un-inoculated medium served as the blank control, and set up three parallel experimental groups. Polysaccharide content was determined by the phenol-sulfuric acid method at 0, 2, 4, 6, 8, 10, and 12 d.

After 12 d, the fermentation liquid was filtered under suction, and the filtrate was centrifuged at 4,000 rpm for 20 min. The supernatant was concentrated to 1/10 of its original volume by Rotary Evaporator (55 °C, 0.1 MPa), followed by protein removal using the Sevage method. Three volumes of ethanol were added, and the mixture was kept at 4 °C for 24 h to precipitate polysaccharides. The precipitate was collected by centrifuge at 4,000 rpm for 20 min, dissolved in 10 ml of distilled water, and dialyzed for 24 h using a 1000 Da dialysis bag (with water changed every 4 h). After dialysis and lyophilization, the polysaccharide yield was calculated according to Formula (1).

The polysaccharide yield (Yield, mg/g) was defined as the total mass of purified polysaccharides obtained from the entire fermentation broth after complete extraction and purification (including Sevage deproteinization, ethanol precipitation, dialysis, and lyophilization), relative to the initial dry mass of corn stalks. To account for volume changes during purification, an aliquot of the fermentation broth containing a known amount of polysaccharides was subjected to the same purification steps. The mass of polysaccharides obtained from this aliquot was then scaled up to represent the total recovery from the entire fermentation broth. The yield was calculated using the following formula:

$$\text{Yield (mg/g)} = \frac{m_1}{m_0} \tag{1}$$

where m_0 = mass of corn stalk added to the fermentation medium (g) and m_1 = calculated total mass of polysaccharides recoverable from the entire fermentation broth (mg).

The polysaccharides from the blank control group were designated as CSP-B (corn straw polysaccharides-blank group), while those from the experimental group were designated as CSP-T (corn straw polysaccharides-test group).

Polysaccharide identification

Using the Molish reaction, phenol-sulfuric acid reaction, Fehling reaction, and iodine-potassium iodide reaction, polysaccharides were identified [8]. CSP-B and CSP-T polysaccharides were each prepared as aqueous solutions at a concentration of 1 mg/ml. These solutions were scanned using a UV-Visible spectrophotometer in the range of 185–800 nm.

Structural changes of corn stalks

The structural changes in corn stalks before and after degradation were analyzed by SEM and FTIR.

Polysaccharide structural characterization

Monosaccharide composition of polysaccharides was determined using HPLC. Structural characterization of polysaccharides was conducted using AFM, SEM, FTIR, iodine-potassium iodide experiment, and Congo red test.

Thermogravimetric analysis of polysaccharides

Thermogravimetric analysis (TGA) of polysaccharides was conducted.

Determination of the hypoglycemic activity of polysaccharides in vitro

1. Determination of the inhibitory activity of polysaccharides on α-amylase:

30 µl polysaccharide solution at varying concentrations (1.0–10.0 mg/ml, prepared in PBS) was mixed with 30 µl of α-amylase solution and incubated at 37 °C for 10 min. Subsequently, 30 µl of soluble starch solution was added, and the reaction was allowed to proceed for an additional 10 min. The reaction was terminated by adding 50 µl of DNS, followed by heating in a boiling water bath for 5 min. After rapid cooling, 500 µl of distilled water was added, and the absorbance was measured at 540 nm. Acarbose was used as the positive control, and the α-amylase inhibition rate was calculated according to Formula (2).

$$\text{α-amylase inhibition rate (\%)} = \left(1-\frac{A_1-A_2}{A_3}\right)\times 100 \quad (2)$$

where A_1 = absorbance at 540 nm of the reaction mixture containing polysaccharide solution and α-amylase solution after incubation; A_2 = absorbance at 540 nm of the sample solution blank; and A_3 = absorbance at 540 nm of the α-amylase solution blank.

2. Determination of the inhibitory activity of polysaccharides on α-glucosidase:

40 µl of polysaccharide solutions at different concentrations (1.0–10.0 mg/ml prepared in PBS) were added to a 96-well plate, followed by the addition of 40 µl of α-glucosidase solution. After mixing, the plate was incubated in a 37 °C Electric thermostatic drying oven for 10 min. Subsequently, 40 µl of PNPG solution was added, and the plate was further incubated at 37 °C for another 10 min. After the incubation period, 100 µl of sodium carbonate solution was added to stop the reaction and develop color for 5 min. The absorbance was measured at a wavelength of 405 nm using a spectrophotometer. Acarbose was used as the positive control. The inhibition rate of α-glucosidase was calculated according to formula (3).

$$\text{α-glucosidase inhibition rate (\%)} = \left(1-\frac{A_1-A_2}{A_3}\right)\times 100 \quad (3)$$

where A_1 = absorbance at 405 nm of the mixture of polysaccharide solution and α-glucosidase solution after reaction; A_2 = absorbance at 405 nm of the sample solution blank; A_3 = absorbance at 405 nm of the α-glucosidase solution blank.

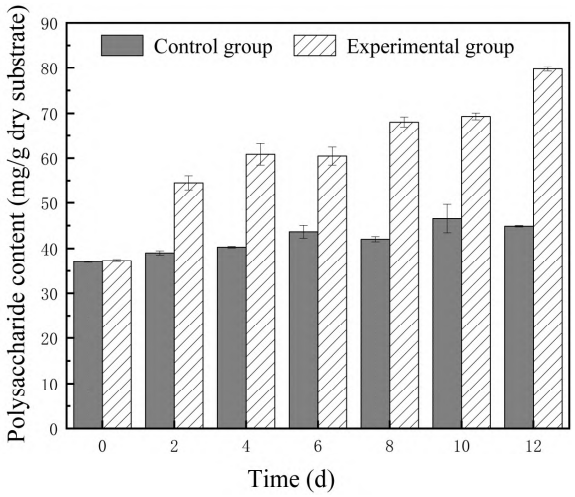

Fig. 1 Polysaccharide content in fermentation broth (per g dry substrate).

RESULTS AND DISCUSSION

Fermentation

Polysaccharide content during fermentation was monitored using the phenol-sulfuric acid method (using glucose as a standard; $R^2 = 0.9997$). The measured concentrations were converted to "mg polysaccharide per g dry substrate (mg/g)" based on the initial dry mass of corn stalks (m_0) and the total fermentation broth volume. As shown in Fig. 1, both the control and experimental groups exhibited an initial polysaccharide content of 37.2 ± 0.2 mg/g at 0 d, likely resulting from the release of hemicellulose and cellulose during corn stalk pretreatment and medium sterilization [9]. After 4 d, the control group showed a slight increase (potentially associated with shaking cultivation), whereas the experimental group demonstrated a significant rise from 2 d onward, reaching 79.8 ± 0.6 mg/g at 12 d (approximately twice the initial value). These results indicate that the elevated polysaccharide content in the experimental group primarily resulted from the degradation of corn stalks by *S. rochei se-93*. The inoculation of *S. rochei se-93* effectively enhanced polysaccharide content in the fermentation broth.

Polysaccharide identification

CSP-B and CSP-T were identified using the Molisch reaction, phenol-sulfuric acid reaction, Fehling's reaction, and iodine-potassium iodide reaction. Upon the addition of the Molisch reagent, CSP-B and CSP-T exhibited red-violet rings, indicating positive Molisch reactions for both substances. In the phenol-sulfuric acid reaction, CSP-B and CSP-T both produced orange-yellow compounds, confirming positive results for this test as well. These outcomes suggested that CSP-B and CSP-T were carbohydrate compounds. In the Fehling

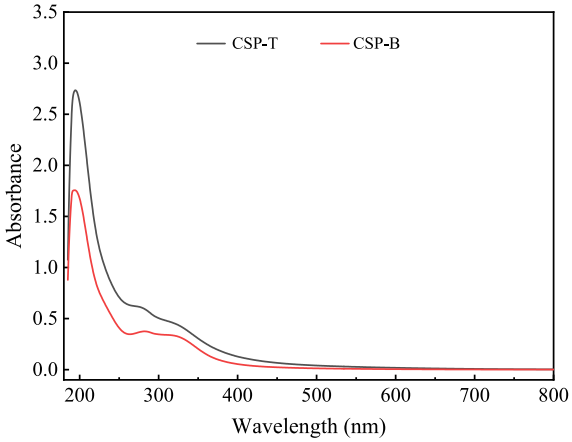

Fig. 2 UV-Visible absorption spectrum for CSP-B and CSP-T.

reaction, neither CSP-B nor CSP-T produced a brick-red precipitate, indicating the absence of reducing sugars in these samples. Similarly, in the iodine-potassium iodide reaction, neither CSP-B nor CSP-T turned blue, suggesting that CSP-B and CSP-T were non-starch polysaccharides.

The UV scanning results for CSP-B and CSP-T are shown in Fig. 2. As depicted in the figure, both CSP-B and CSP-T exhibited a minor absorption peak around 280 nm, which was primarily attributed to the presence of proteins. Additionally, both CSP-B and CSP-T displayed strong absorption peaks around 200 nm, characteristic of polysaccharides [10]. This further confirmed that the main components of CSP-B and CSP-T were carbohydrate substances. The UV scanning results indicated that the polysaccharide purity of CSP-B and CSP-T was relatively high.

Structural changes of corn stalks

The microstructural changes in corn stalks post-fermentation were observed using SEM. From Fig. 3(A), it was evident that the surface of corn stalk fragments in the control group appeared smooth and densely structured, with small cracks likely resulting from physical processes such as fragmentation and oscillation during cultivation. In contrast, the corn stalks in the experimental group exhibited serrated erosion marks, distinct cracks, and holes on the surface, indicating significant structural damage. This suggests that *S. rochei se-93* effectively degrades corn stalks, likely via enzymes secreted during microbial growth and metabolism [11].

The FTIR spectra of corn stalks from the post-fermentation control group and experimental group are shown in Fig. 3(B). The absorption peak at 3344 cm^{-1} corresponded to the stretching vibration of —OH groups [12]. The experimental group exhibited a lower intensity at this peak compared to the control group, indicating the disruption of hydrogen bonds in cellulose fibers due to fermentation with *S. rochei se-93* [13]. The peaks at 2905 cm^{-1} and 1730 cm^{-1} represented the stretching vibrations of methyl and methylene groups [14] and the C=O stretching vibration in hemicellulose [15], respectively. The peaks at 1166 cm^{-1} and 1054 cm^{-1} indicated the presence of C—O—C bonds [16]. The decreased intensity of these vibrational peaks suggested partial degradation of cellulose and hemicellulose in the corn stalks of the experimental group [17].

The absorption peak near 1250 cm^{-1} corresponded to the C=O stretching vibration in lignin. The reduced absorption intensity at this point in the experimental group indicates a decrease in lignin content in corn stalks due to microbial fermentation [18]. These results demonstrated that during fermentation, *S. rochei se-93* effectively degraded cellulose, hemicellulose, and lignin in the corn stalks.

Characterization of polysaccharide structures

SEM and AFM analysis

Fig. 4(a,b,c,d) displays the SEM images of CSP-B and CSP-T. The images revealed that while the surface morphology of CSP-B and CSP-T showed no significant difference, there were subtle distinctions. Under 1,000 × magnification (a,c), CSP-B and CSP-T appeared as clusters of spherical particles forming blocky structures. However, the arrangement of CSP-T was denser than that of CSP-B, with smaller interparticle gaps. At 10,000 × magnification (b,d), CSP-B exhibited a more uniform particle size distribution with loosely arranged particles, while CSP-T showed a varied particle size distribution with closely packed particles. These morphological changes may be attributed to the partial degradation of lignin and hemicellulose, which releases specific phenolic compounds. Phenolic compounds are bound within cellulose and hemicellulose [19], and microbial fermentation facilitates the degradation of lignin and hemicellulose, thereby releasing these phenolic compounds [20]. Upon oxidation, these phenolic compounds generate highly reactive intermediates that undergo oxidative cross-linking with polysaccharide chains, leading to tighter packing of polysaccharide particles [21].

As shown in Fig. 4(e,f,g,h), within a 5.0 × 5.0 μm field of view, CSP-B and CSP-T exhibited unevenly sized spherical structures, indicating irregular aggregation in aqueous solutions at room temperature, with entangled molecular interactions. Analysis of the heights of polysaccharide chains of CSP-B and CSP-T reveals a range from 0.3 to 25.0 nm. CSP-T demonstrates a higher degree of aggregation compared to CSP-B, consistent with a more compact surface morphology observed in subsequent SEM images. Studies suggested that the height of a single polysaccharide chain typically fell within the range of 0.1–1.0 nm [22]. The observed heights of CSP-B and CSP-T in AFM images

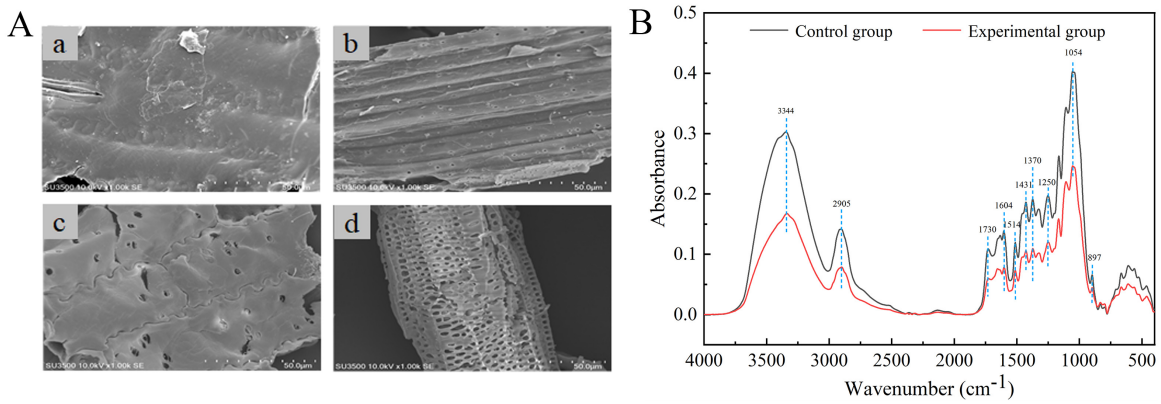

Fig. 3 (A) SEM analysis (a,b,c,d) and (B) FTIR spectrum of corn stalks after the degradation. Note: (a,b) represented the SEM images of corn stalks in the control group; (c,d) represented the SEM images of corn stalks in the experimental group.

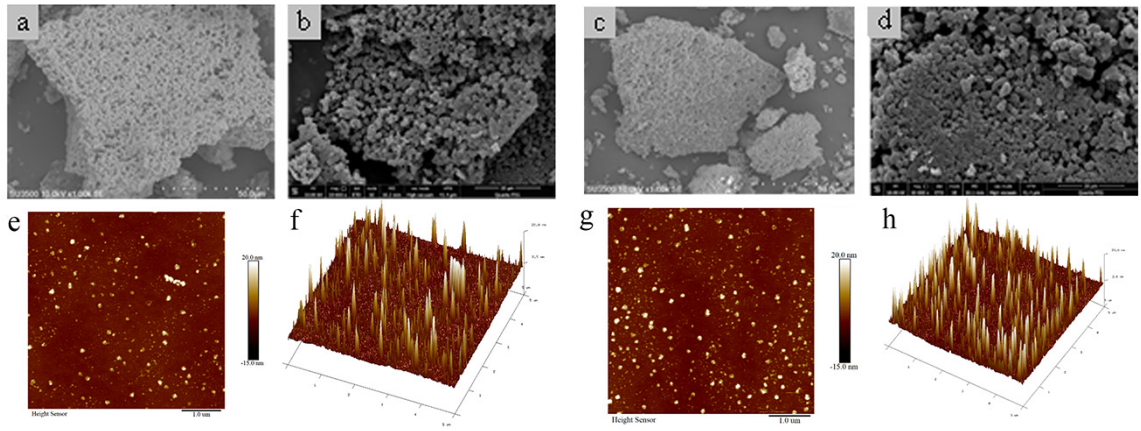

Fig. 4 SEM and AFM images of CSP-B and CSP-T. Note: (a,b) SEM images of CSP-B; (c,d) SEM images of CSP-T; (e) Plan diagram and (f) 3-dimensional stereo diagram of AFM images of CSP-B; (g) Plan diagram and (h) 3-dimensional stereo diagram of AFM images of CSP-T.

far exceeded this range, indicating that CSP-B and CSP-T were capable of crosslinking with multiple single chains. This may have occurred through the formation of hydrogen bonds between or within molecules, leading to entanglement of sugar chains, or through van der Waals forces between polysaccharide molecules [23].

Monosaccharide composition of polysaccharides

The monosaccharide composition of CSP-B and CSP-T was determined using pre-column derivatization with PMP (1-phenyl-3-methyl-5-pyrazolone). The monosaccharide composition and percentages of CSP-B and CSP-T are shown in Fig. 5(b,c). Both CSP-B and CSP-T contained mannose, ribose, rhamnose, glucuronic acid, galacturonic acid, glucose, galactose, xylose, and arabinose. The percentage composition of each monosaccharide in CSP-B was as follows: 0.27%, 0.03%, 8.65%, 0.96%, 2.20%, 1.90%, 0.76%, 0.56%, and 84.67%. In CSP-T, the percentages were 2.37%, 0.27%, 0.32%, 8.15%, 2.05%, 0.19%, 0.17%, 0.47%, and 86.01%. Arabinose was the predominant monosaccharide in both polysaccharides, accounting for 84.67% in CSP-B and 86.01% in CSP-T. The high proportion of arabinose in CSP-B may be attributed to the following reasons: corn stalks are rich in arabinoxylan, a type of hemicellulose primarily composed of arabinose and xylose [24]. Since CSP-B is mainly derived from water-soluble or easily extractable polysaccharides in the raw material, it retains a relatively high arabinose content. Additionally, the pretreatment of corn stalks before fermentation may lead to the partial dissolution of hemicellulose, further increasing the relative arabinose content in the extract [25]. The contents of ribose, galactose, and xylose were lower. The glucuronic acid content in CSP-T (8.15%) was significantly higher than in CSP-B (0.96%). This change in composition is expected to significantly enhance the solubility and viscosity of the polysaccharide. The ionizable carboxyl groups improve water solubility

and chain expansion, which likely contributes to its improved bioactivity by increasing bioavailability and modulating interactions with biological targets [26, 27]. Furthermore, the increased uronic acid content may alter the rheological properties of the polysaccharide solution, potentially leading to higher viscosity, a feature often associated with the bioactivity of certain polysaccharides [28]. The composition of monosaccharides remained unchanged after the addition of microorganisms, but their proportions shifted. This shift can likely be attributed to the ability of *Streptomyces* to secrete various enzymes during fermentation, which more efficiently degrade corn stalks, releasing additional monosaccharides and thereby altering their relative proportions [29].

FTIR spectroscopy of polysaccharides

Fig. 5(d) shows the infrared absorption spectra of CSP-B and CSP-T within the range of 4000–400 cm^{-1}. Both CSP-B and CSP-T exhibited a prominent absorption peak around 3414 cm^{-1}, attributed to the stretching vibration of polysaccharide hydroxyl groups and a weaker absorption peak at 2932 cm^{-1} was related to the C—H stretching vibration of polysaccharide alkyl groups [30]. The typical groups of polysaccharides, hydroxyl and alkyl, appeared in both CSP-B and CSP-T, indicating that both CSP-B and CSP-T were polysaccharides. The absorption peak near 1613 cm^{-1} was due to the asymmetric stretching vibration of C=O bonds [31], while the peak at 1512 cm^{-1} arose from the stretching vibration of the polysaccharide phenyl ring. The peak at 1386 cm^{-1} corresponded to the bending vibration of O—H groups, and the absorptions near 1000–1200 cm^{-1} were attributed to the stretching vibration of C—O—C bonds on the pyranose ring [32].

Both CSP-B and CSP-T exhibited peaks at 1086 cm^{-1}, indicating a pyranose sugar-type structure. The absorption peak at 865 cm^{-1} indicated the presence of β-glycosidic bonds in CSP-B and CSP-T [33].

In summary, both CSP-B and CSP-T are composed of pyranose-type structures featuring β-glycosidic bonds. These results demonstrated that the introduction of *S. rochei se-93* enhanced the extraction yield of polysaccharides without altering their functional groups and configurations.

Analysis of polysaccharides by iodine-potassium iodide reaction

The iodine-potassium iodide reaction is used to study the branching and side-chain characteristics of polysaccharides. The principle of this experiment is that when the iodine reagent is mixed with polysaccharides that have minimal branching or shorter side chains, the iodine reagent cannot form complexes with these polysaccharides. In UV scans, this results in a maximum absorption peak at 565 nm. Conversely, when the iodine solution is mixed with polysaccharides that have more branching or longer side chains, the increased number of binding sites allows iodine to form complexes with these polysaccharides, causing a blue shift in the maximum absorption peak [34].

Fig. 5(e) shows the iodine-potassium iodide reaction results for CSP-B and CSP-T. As shown in the figure, CSP-B and CSP-T exhibited distinct absorption peaks at 348 nm and 346 nm, respectively, with no absorption peaks at 565 nm indicating the presence of longer side chains and more branching in CSP-B and CSP-T [34].

Analysis of polysaccharides by Congo red reaction

Congo red is an acidic dye commonly used in chemical quantification and qualitative analyses. It reacts with polysaccharides exhibiting a triple-helical conformation in an alkaline environment, forming complexes that exhibit a red shift in the maximum absorption wavelength compared to Congo red alone [35]. This study conducted Congo red experiments on CSP-B and CSP-T to confirm the presence of triple-helical structures in these polysaccharides. As shown in Fig. 5(f), the maximum absorption wavelengths of the Congo red + CSP-B and Congo red + CSP-T solutions exhibited significant red shifts compared to the Congo red solution alone, indicating that the triple-helical structures in CSP-B and CSP-T formed complexes with Congo red. Therefore, CSP-B and CSP-T both possessed triple-helical structures.

Thermogravimetric analysis of polysaccharides

The thermal degradation curves of CSP-B and CSP-T exhibited three main stages.

In the first stage, CSP-B showed a temperature range from room temperature to 200 °C, with a mass loss rate of 10.12%. This mass loss was primarily due to the physical adsorption of free water in the polysaccharide, indicating good stability of CSP-B within this temperature range. CSP-T's first stage ranged from room temperature to 190 °C, with a mass loss rate of 8.60%, showing an earlier peak temperature loss of 10 °C compared to CSP-B.

The second stage for CSP-B and CSP-T ranged from 200–550 °C and 190–495 °C, with mass loss rates reaching 37.22% and 44.21%, respectively. This stage exhibited the most significant polysaccharide degradation, indicating intense decomposition within this temperature range. The primary reasons for weight loss in this stage were likely due to the rupture of carbon chains, polysaccharide degradation, and the formation of volatile components from thermal decomposition [36].

In the third stage, CSP-B and CSP-T ranged from 550–800 °C and 490–800 °C, respectively. In this stage, the weight of polysaccharides tended to change gently, and the mass loss rates of CSP-B and CSP-T were 7.90% and 5.48%, respectively. The decomposition rate of polysaccharides slowed down at this stage, which may have been due to the carbonization of polysaccharides [37].

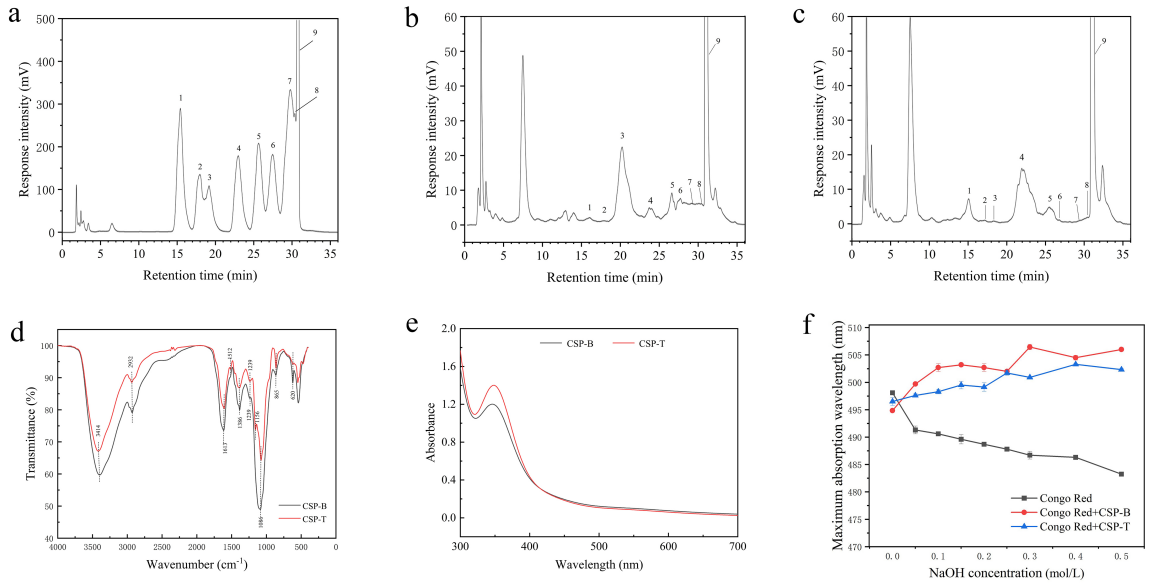

Fig. 5 HPLC chromatograms of (a) to (c): mixed standard monosaccharide derivatives (a), and monosaccharide compositions of CSP-B (b) and CSP-T (c); FT-IR spectra (d) and Iodine-potassium iodide reaction diagram (e) of CSP-B and CSP-T; and changes in the maximum absorption wavelengths of CSP-B and CSP-T in the Congo red reaction (f). Note: in (a,b,c) 1, 2, 3, 4, 5, 6, 7, 8, and 9 represent Man, Rib, Rha, GlcUA, GalUA, Glc, Gal, Xyl, and Ara, respectively.

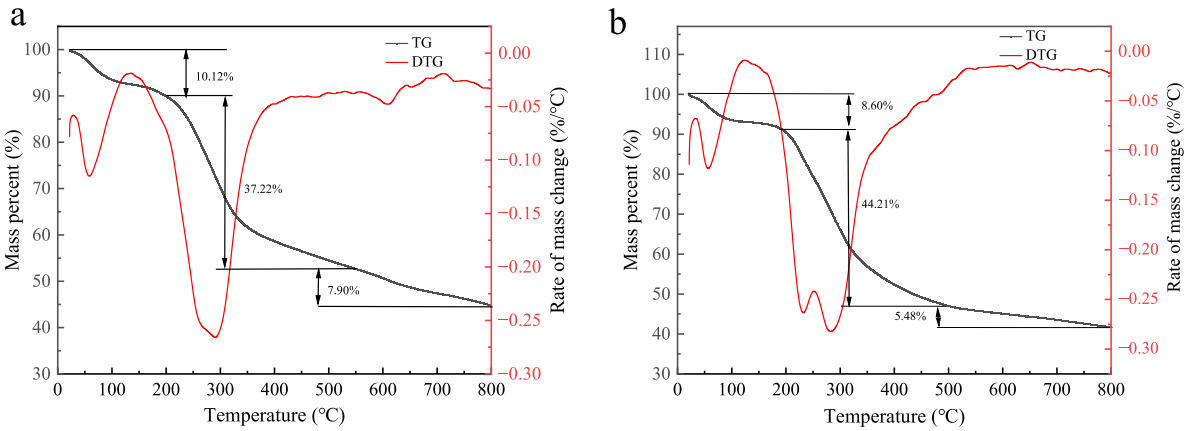

Fig. 6 TG and DTG curves of CSP-B (a) and CSP-T (b).

Overall, the total weight loss rates of CSP-B and CSP-T reached 55.26% and 58.29%, respectively. Both polysaccharides remained stable from room temperature up to 190 °C, indicating good thermal stability [23]. However, CSP-T showed slightly lower thermal stability compared to CSP-B, suggesting that the fermentation by *S. rochei se-93* reduced the thermal stability of the polysaccharides.

In vitro hypoglycemic activity of polysaccharides

Similar to other metabolic enzymes, α-amylase and α-glucosidase rapidly increase blood glucose levels in the human body by degrading carbohydrates [38]. Therefore, regulating carbohydrate digestion by inhibiting the activities of α-amylase and α-glucosidase was an effective strategy for preventing hyperglycemia [39]. This study investigated the inhibitory effects of polysaccharides CSP-B and CSP-T on α-amylase and α-glucosidase, as shown in Fig. 7(a).

The inhibitory effects of CSP-B and CSP-T on α-amylase activity are depicted in Fig. 7. Both CSP-B and CSP-T exhibited inhibitory effects on α-amylase activity, although their effectiveness was lower than that of the positive control, acarbose. Within the polysaccharide concentration range of 1–10 mg/ml, CSP-T showed the highest inhibition at a concentration of 2 mg/ml, achieving 56.90 ± 0.42%. However, the inhibitory effect decreased as the concentration increased beyond 2 mg/ml. CSP-B reached its maximum inhibition rate of 54.43 ± 0.28% at a concentration of

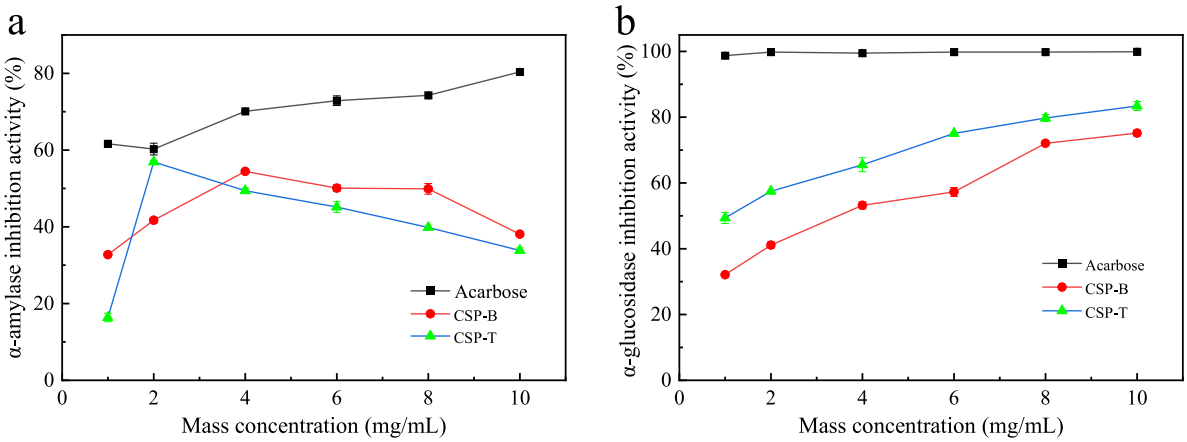

Fig. 7 α-amylase (a) and α-glucosidase (b) inhibitory activities of polysaccharides CSP-B and CSP-T.

4 mg/ml. CSP-T demonstrated a characteristic of high efficiency at low doses in inhibiting α-amylase activity compared to CSP-B.

The inhibitory effects of CSP-B and CSP-T on α-glucosidase activity are illustrated in Fig. 7(b). Acarbose, serving as a positive control, exhibited a high inhibition rate even at lower concentrations. The inhibition effects of CSP-B and CSP-T on α-glucosidase activity were dose-dependent. At a polysaccharide concentration of 10 mg/ml, the inhibition rates of CSP-B and CSP-T on α-glucosidase reached their peak values, at 75.16 ± 0.91% and 83.40 ± 1.36%, respectively. The inhibition trends of CSP-B and CSP-T were similar at each measured concentration point; however, CSP-T showed stronger inhibitory activity than CSP-B. This enhanced inhibitory effect of CSP-T was likely due to its significantly higher content of glucuronic acid compared to CSP-B, which enhanced the polysaccharide's inhibitory action on α-glucosidase activity [40].

The enzyme inhibition assay used in this study has certain limitations. Although we performed systematic background correction by including sample and enzyme blanks, and validated the experimental system using acarbose, the absence of a heat-inactivated enzyme control means that interference from non-enzymatic hydrolysis cannot be fully ruled out. This aspect should be addressed in future studies. Nevertheless, the data obtained demonstrate a clear dose-dependent inhibitory effect, with a response trend consistent with that of the standard inhibitor, providing preliminary evidence that CSP-B and CSP-T may act as potential α-amylase/α-glucosidase inhibitors.

CONCLUSION

This study investigated the liquid fermentation of corn stalk by *S. rochei se-93* to extract polysaccharide CSP-T, which was then compared with the polysaccharide CSP-B extracted from the control group. The results demonstrate that *S. rochei se-93* effectively utilized corn stalk for polysaccharide production, yielding a content of 79.8 ± 0.6 mg/g after 12 d of fermentation, twice the initial level. Both CSP-B and CSP-T were identified as pyranose-type polysaccharides with β-glycosidic bonds, sharing the same monosaccharide composition but differing in their proportions. CSP-T exhibited a significant increase in glucuronic acid content, a more compact structure, and slightly reduced thermal stability. In addition, CSP-B and CSP-T demonstrated potential inhibitory activity against both α-amylase and α-glucosidase. The underlying mechanism may involve the binding of active structural motifs to the enzymes active sites, thereby competitively inhibiting enzymesubstrate interactions. The maximum inhibition rates of CSP-B and CSP-T on against α-amylase were 56.90 ± 0.91% (4 mg/ml) and 54.43 ± 0.28% (2 mg/ml), respectively. Meanwhile, their maximum inhibition rates on α-glucosidase reached 75.16 ± 0.91% (10 mg/ml) and 83.40 ± 1.36% (10 mg/ml), respectively. The study indicates that fermentation by *S. rochei se-93* enhanced the hypoglycemic activity of polysaccharides, suggesting that CSP-T has good potential as a natural source of α-glucosidase inhibitors.

Acknowledgements: This research was partially supported by Tianjin Science and Technology Planning Project (22YDTPJC00760), Tianjin Key R&D Program-Social Development and Agriculture Project (21YFSNSN00190) and Tiankai Higher Education Science and Technology Innovation Park R&D Program (23YFZXYC00019).

REFERENCES

1. Chen L, Huang L (2024) Protective effect and mechanisms of *Chimonanthus salicifolius* polysaccharide on acute alcoholic liver injury in mice. *ScienceAsia* **50**, ID 2024112.
2. Xue L, Yang R, Ma G, Li G, Li W, Mo T (2017) Progress in research of straw biodegradation mechanisms and functional microbial flora. *Ecol Sci* **36**, 193–199.

3. Zhang J, Qian YT, Qu P, Cao Y, Wang QJ, Huang HY (2023) Screening, identification and degradation characteristics of one straw degrading actinomycete strain. *J China Agric Univ* **28**, 75–83.
4. Wang WW, Wu JJ, Yang XL, Li YH, Feng X, Xie YH (2022) Process optimization of polysaccharide production by microbial fermentation with corn stalks as substrate. *J Agric Resour Environ* **50**, 194–197.
5. Gong X, Yu Y, Hao Y, Wang Q, Ma J, Jiang Y, Lv G, Li L, et al (2022) Characterizing corn-straw-degrading actinomycetes and evaluating application efficiency in straw-returning experiments. *Front Microbiol* **13**, 1003157.
6. Wang JJ, Xi YL, Chang ZZ, Wang MY, Zhang R (2015) The differences of biodegradation rates in the different parts of wheat straw. *J Agric Resour Environ* **32**, 74–80.
7. Jin XC, Wu GF, Sun EH, Tang WY, Huang HY, Chen L (2017) Improving processability of rice straw by fermentation using *Streptomyces rochei*. *J Nanjing For Univ* **41**, 122–128.
8. Zhao X, Wang Y, Liu Q, An W (2008) Extraction technology and physicochemical properties of *Cornus officinalis* polysaccharides. *Lishizhen Med Mater Med Res*, 1597–1599.
9. Shen YY, Qin XX, Teng QM (2019) Determination of protein content in *Eleocharis dulcis* polysaccharides. *Stud Trace Elem Health* **36**, 50–52.
10. Li Y, Guo M, Shao J, Sang Y, Sun J (2023) Chemical composition, physicochemical properties and hypoglycemic activity *in vitro* of polysaccharide from loach (*Paramisgurnus dabryanus*) mucus. *J Chin Inst Food Sci Technol* **23**, 51–62.
11. Yao L, Zhao J, Xie YM, Yang H, Yang W, Qu Y (2012) Mechanism of diluted acid pretreatment to improve enzymatic hydrolysis of corn stover. *Chem Ind For Prod* **32**, 87–92.
12. Guo F, Altaner CM (2018) Molecular deformation of wood and cellulose studied by near infrared spectroscopy. *Carbohydr Polym* **197**, 1–8.
13. Su Y, Yu X, Sun Y, Wang G, Chen H, Chen G (2018) Evaluation of screened lignin-degrading fungi for the biological pretreatment of corn stover. *Sci Rep* **8**, 5385.
14. Liu JQ, Guo J, Wu AL, Dong EW, Wang JS, Wang LG, Jiao XY (2019) Study on infrared spectroscopy of decomposition process of sorghum and corn straw. *J Shanxi Agric Sci* **47**, 387–392.
15. Jin X, Chen X, Shi C, Li M, Guan Y, Yu CY, Yamada T, Sacks EJ, et al (2017) Determination of hemicellulose, cellulose and lignin content using visible and near infrared spectroscopy in *Miscanthus sinensis*. *Bioresour Technol* **241**, 603–609.
16. Khan AS, Man Z, Bustam MA, Nasrullah A, Ullah Z, Sarwono A, Shah FU, Muhammad N (2018) Efficient conversion of lignocellulosic biomass to levulinic acid using acidic ionic liquids. *Carbohydr Polym* **181**, 208–214.
17. Li HY, Li SN, Wang SX, Wang Q, Xue YY, Zhu BC (2015) Degradation of lignocellulose in the corn straw by *Bacillus amyloliquefaciens* MN-8. *Chin J Appl Ecol* **26**, 1404–1410.
18. Owolabi AF, Haafiz MKM, Hossain MS, Hussin MH, Fazita MRN (2017) Influence of alkaline hydrogen peroxide pre-hydrolysis on the isolation of microcrystalline cellulose from oil palm fronds. *Int J Biol Macromol* **95**, 1228–1234.
19. Acosta-Estrada BA, Gutiérrez-Uribe JA, Serna-Saldívar SO (2014) Bound phenolics in foods, a review. *Food Chem* **152**, 46–55.
20. Jamal P, Idris ZM, Alam MZ (2011) Effects of physicochemical parameters on the production of phenolic acids from palm oil mill effluent under liquid-state fermentation by *Aspergillus niger* IBS-103ZA. *Food Chem* **124**, 1595–1602.
21. Nadar SS, Rao P, Rathod VK (2018) Enzyme assisted extraction of biomolecules as an approach to novel extraction technology: A review. *Food Res Int* **108**, 309–330.
22. Kiriy A, Gorodyska G, Minko S, Tsitsilianis C, Jaeger W, Stamm M (2003) Chemical contrasting in a single polymer molecule AFM experiment. *J Am Chem Soc* **125**, 11202–11203.
23. Chen Y, Ping H, Gao Y, Du Y, Liu J, Zhang L (2024) Isolation, purification, structure characterization and antibacterial activity of polysaccharides from proso millet bran. *Sci Technol Food Ind* **45**, 1–7.
24. Weng V, Cardeira M, Bento-Silva A, Serra AT, Brazinha C, Bronze MR (2023) Arabinoxylan from corn fiber obtained through alkaline extraction and membrane purification: relating bioactivities with the phenolic compounds. *Molecules* **28**, 5621.
25. Liu D, Tang W, Yin JY, Nie SP, Xie MY (2021) Monosaccharide composition analysis of polysaccharides from natural sources: hydrolysis condition and detection method development. *Food Hydrocoll* **116**, 106641.
26. Li Z, Wei Y, Wang Y, Zhang R, Zhang C, Wang C, Yan X (2022) Preparation of highly substituted sulfated alfalfa polysaccharides and evaluation of their biological activity. *Foods* **11**, 737.
27. Baghel M, Sakure K, Giri TK, Maiti S, Nakhate KT, Ojha S, Sharma C, Agrawal Y, et al (2023) Carboxymethylated gums and derivatization: strategies and significance in drug delivery and tissue engineering. *Pharmaceuticals* **16**, 776.
28. Wang Z, Zheng Y, Lai Z, Hu X, Wang L, Wang X, Li Z, Gao M, et al (2024) Effect of monosaccharide composition and proportion on the bioactivity of polysaccharides: A review. *Int J Biol Macromol* **254**, 127955.
29. Kashiwagi N, Ogino C, Kondo A (2017) Production of chemicals and proteins using biomass-derived substrates from a Streptomyces host. *Bioresour Technol* **245**, 1655–1663.
30. Zhang Z, Guo L, Yan A, Feng L, Wan Y (2020) Fractionation, structure and conformation characterization of polysaccharides from *Anoectochilus roxburghii*. *Carbohydr Polym* **231**, 115688.
31. Zheng CC, Li T, Tang YY, Lu T, Wu MK, Sun J, Man RJ, He XM, et al (2024) Structural and functional investigation on stem and peel polysaccharides from different varieties of pitaya. *Int J Biol Macromol* **259**, 129172.
32. Zhang Q, Xu Y, Lv J, Cheng M, Wu Y, Cao K, Zhang X, Mou X, et al (2018) Structure characterization of two functional polysaccharides from *Polygonum multiflorum* and its immunomodulatory. *Int J Biol Macromol* **113**, 195–204.
33. Liao W, Luo Z, Liu D, Ning Z, Yang J, Ren J (2015) Structure characterization of a novel polysaccharide from *Dictyophora indusiata* and its macrophage immunomodulatory activities. *J Agric Food Chem* **63**, 535–544.

34. Wen QH, Lu YH, Yang LF, Chen JX, Cheng YY, Liu Y, Xu S, Ma FW (2024) Preparation, structure characterization and antioxidant activity evaluation of selenized *Gastrodia elata* polysaccharides. *Sci Technol Food Ind* **45**, 18–30.
35. Huang Y, Xie W, Tang T, Chen H, Zhou X (2023) Structural characteristics, antioxidant and hypoglycemic activities of polysaccharides from *Mori Fructus* based on different extraction methods. *Front Nutr* **10**, 1125831.
36. Zhang H, Li H, Netala VR, Hou T, Zhang Z (2022) Optimization of complex enzyme-ultrasonic synergistic extraction of water-soluble polysaccharides from *Perilla frutescens* seed meal: purification, characterization and *in vitro* antioxidant activity. *J Food Process Preserv* **46**, e16201.
37. Xing HZ, Zhang YM, Liu HP, Qiao SF (2023) Preparation, thermal stability and antioxidant activity of polysaccharide from *Lophatherum gracile* Brongn. *Food Res Dev* **44**, 86–96.
38. Cui M, Cheng L, Shen Y, Liu K, Liu K (2023) Structural characterization, hypoglycemic and immune-enhancing activities of a polysaccharide from *Oenanthe javanica*. *J Food Meas Charact* **17**, 6318–6329.
39. Duan WX, Yang XH, Zhang HF, Feng J, Zhang MY (2022) Chemical structure, hypoglycemic activity, and mechanism of action of selenium polysaccharides. *Biol Trace Elem Res* **200**, 4404–4418.
40. Nie C, Zhu P, Wang M, Ma S, Wei Z (2017) Optimization of water-soluble polysaccharides from stem lettuce by response surface methodology and study on its characterization and bioactivities. *Int J Biol Macromol* **105**, 912–923.